Green Chemical Engineering 6 (2025) 562–571

Contents lists available at ScienceDirect

Green Chemical Engineering

journal homepage: www.keaipublishing.com/en/journals/green-chemical-engineering

Article

Aqueous polyamine-based deep eutectic solvent: balancing stability, CO_2 absorption/desorption performance, and post-absorption viscosity

Kaige Jia, Qiangbing Shi, Xiaoyan Ji *

Division of Energy Science/Energy Engineering, Luleå University of Technology, Luleå, 97187, Sweden

HIGHLIGHTS

- A novel aqueous polyamine-based DES ([PzCl][DETA]) system was designed and synthesized.
- A systematic evaluation and performance optimization of the DES system was conducted.
- The selected solvent outperformed MEA in both performance metrics and industrial feasibility.
- The results provided practical guidance for scalable CO_2 absorbent development.

GRAPHICAL ABSTRACT

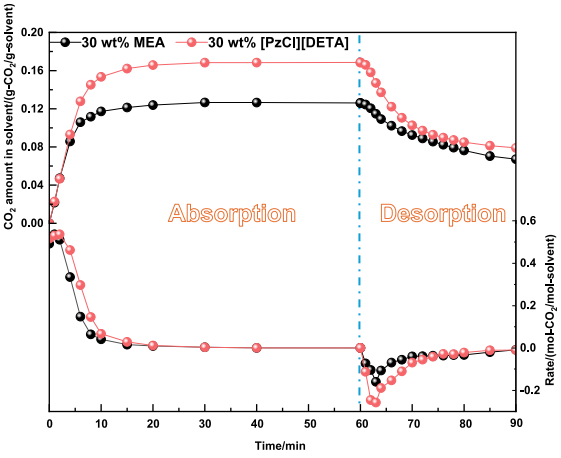

ARTICLE INFO

Keywords:
Deep eutectic solvent
CO_2 absorption
Desorption efficiency
Viscosity

ABSTRACT

Deep eutectic solvents (DESs) have gained significant attention as potential absorbents for CO_2 capture due to their tunable physicochemical properties and environmental sustainability. However, achieving a balance of thermal stability, absorption/desorption performance, and viscosity remains a critical challenge for industrial applications. To address this, a novel aqueous polyamine-based DES system was developed using an ionic liquid with high stability–PzCl (piperazine chloride, P), as a hydrogen bond acceptor (HBA); a polyamine with multiple active sites, DETA (diethylenetriamine, D), as a hydrogen bond donor (HBD), and H_2O as co-solvent. By systematically optimizing the molar ratio of PzCl to DETA, [PzCl][DETA] (PD) with a 1:5 molar ratio was identified as the optimal one based on the absorption capacity/rate, thermal stability, post-absorption viscosity, and desorption efficiency of its aqueous solution. Further investigation into the water content revealed that 30 wt% [PzCl][DETA] (1:5) effectively balanced the CO_2 absorption capacity (0.168 g-CO_2/g-absorbent) and desorption efficiency (54%), more outstanding than those of 30 wt% MEA (0.126 g-CO_2/g-absorbent and 47%, respectively), and provided acceptable post-absorption viscosity (8.11 mPa·s), which was slightly higher than that of 30 wt% MEA (3.77 mPa·s) but lower than 10 mPa·s. These findings provide a scalable framework for designing

* Corresponding author.
E-mail address: xiaoyan.ji@ltu.se (X. Ji).

https://doi.org/10.1016/j.gce.2025.06.001
Received 14 April 2025; Received in revised form 24 May 2025; Accepted 2 June 2025
Available online 5 June 2025

sustainable absorbents that harmonize high performance with operational viability. This work bridges the gap between laboratory-scale innovations and industrial implementation in carbon capture technologies.

1. Introduction

Excessive CO_2 emissions have become a primary driver of global climate change and ecological imbalance, prompting nations worldwide to accelerate their carbon neutrality efforts. Carbon capture, utilization, and storage (CCUS) technology has emerged as a pivotal strategy for mitigating CO_2 emissions, playing an irreplaceable role in high-emission sectors such as energy and industry [1,2]. Among the various stages of CCUS, carbon capture serves as the foundational step, directly influencing the overall efficiency and cost of CCUS as well as the subsequent CO_2 utilization and storage processes, making it one of the most decisive components within the CCUS framework [3]. Currently, chemical absorption stands out as the most mature and widely adopted carbon capture technology owing to high selectivity, large CO_2 absorption capacity, and suitability for large-scale industrial flue gas streams. The choice of absorbent is the critical factor in this process, directly affecting key performance parameters such as CO_2 mass transfer rate, absorption capacity, energy demand, corrosion behavior, and long-term operational stability, all of which determine the overall techno-economic viability and sustainability of the process. Consequently, the continuous optimization and innovation of absorbents is not only a crucial breakthrough for enhancing the competitiveness of chemical absorption technology but also a driving force for advancing CCUS technology toward greater efficiency, economic feasibility, and environmental sustainability, contributing significantly to the global carbon reduction targets [4].

Chemical absorbents with high application potential for CO_2 capture primarily include aqueous amine solutions, potassium carbonate solutions, ionic liquids (ILs) and IL hybrid solvents, as well as deep eutectic solvents (DESs) and DES hybrid solvents [5,6]. Each of these absorbents possesses distinct characteristics, which influence their suitability for different industrial applications. Among them, aqueous amine solutions, despite their widespread use, face significant challenges in balancing corrosion resistance, absorption rate, and energy demand. Potassium carbonate solutions, although suitable for carbon capture at high temperatures, struggle to achieve substantial improvements in absorption rate [7]. Meanwhile, ILs, despite their adjustable structure, negligible volatility, and high thermal stability, face limitations in cost and viscosity, and the efforts to lower viscosity and costs by adding a co-solvent to form IL hybrid solvents often result in reduced absorption capacity. Under these circumstances, the significantly structural and compositional adaptability makes DES hybrid solvents the ideal absorbents that can integrate the benefits of various types of absorbents, where the hydrogen bond acceptor (HBA), hydrogen bond donor (HBD), and co-solvent can be customized [8–10]. In particular, H_2O is the most commonly used, highly effective, and cost-efficient co-solvent, which can decrease the viscosity without disrupting the original hydrogen-bonding network of DESs at moderate concentrations [11–13]. Additionally, by utilizing the amine-based chemicals as the HBD, DESs can effectively lower costs while maintaining robust absorption capacity, even when mixed with H_2O [11–14]. Afterward, ILs, acting as the HBAs, enhance the stability and promote the regeneration of the corresponding DESs system without substantially increasing the cost due to the relatively small dosage [15]. This combination of characteristics allows aqueous DESs to offer a versatile and efficient solution for CO_2 capture, overcoming the limitations of traditional absorbents and providing a more cost-effective and feasible alternative [4,6,16,17].

Polyamines, including ethylenediamine (EDA), diethylenetriamine (DETA), triethylenetetramine (TETA), and tetraethylenepentamine (TEPA), have been studied as the HBD of DESs due to their significant advantages in the CO_2 absorption. Naser et al. [18] investigated the performance of the DESs consisting of monoethanolamide hydrochloride (MEACl) as the HBA and polyamines as HBDs. The results showed that the DES systems with DETA, TETA, and TEPA as the HBDs in a molar ratio of 1:9 achieved the highest CO_2 solubility of 0.283, 0.206, and 0.172 g-CO_2/g-DES, respectively. Shao et al. [19] explored the CO_2 absorption performance of a novel aqueous DES based on choline chloride (ChCl) and DETA in a rotor-stator reactor (RSR). Their study demonstrated that the ChCl/DETA/H_2O with 1:5:2 molar ratio exhibited a remarkable CO_2 uptake (0.250 g-CO_2/g-DES) in a RSR, along with enhanced absorption efficiency and reaction kinetics. Aroua et al. [20] studied the effect of temperature and pressure on the CO_2 absorption of non-aqueous DES consisting of choline hydroxide (ChOH) as the HBA, DETA and TETA as the HBDs, and dimethylsulfoxide (DMSO) as the co-solvent. The results showed that 2 mol/L ChOH/DETA (1:1) and ChOH/TETA (1:1) in DMSO absorbed up to 0.448 and 0.372 g-CO_2/g-DES at 40 °C and 1.4 MPa, respectively. ILs with chloride anions (Cl^-) are the most common and popular choice as the HBAs for the DES preparation due to their structural simplicity and cost-effective, as well as low toxicity [21,22]. Pandey et al. [23] explored the interaction mechanisms of the DESs using ChCl as the HBA and a range of superbases as the HBDs. Building upon the previous study on high-pressure conditions and various temperatures and molar ratios of HBA to HBD [24], Magueijo et al. [22] further investigated the regeneration performance and CO_2 selectivity of these solvents, as well as the effects of the water content on their absorption-desorption behavior and thermodynamic properties. Piperazine (Pz), another polyamine with extremely low molecular weight, exhibits strong basicity and excellent chemical activity and demonstrates effectiveness in enhancing the CO_2 absorption kinetics and promoting desorption efficiency [25,26], making it an excellent candidate for the cation in the IL.

This work was to design an aqueous DES solution that achieves an optimal balance of thermal stability, CO_2 absorption/desorption performance, and post-absorption viscosity. Chlorinated Pz (piperazine chloride, PzCl) was selected to serve as the HBA to enhance the overall stability; DETA, owing to its polyamine structure and moderate molecular weight, was selected as the HBD to increase the CO_2 absorption capacity; and H_2O was used as a co-solvent to optimize the absorption/desorption kinetics. Based on this strategy, aqueous [PzCl][DETA] (PD) solutions were prepared by adjusting the molar ratio of PzCl to DETA as well as the PD content. Based on a comprehensive performance evaluation, including absorption/desorption performance and viscosity before and after absorption, the optimal aqueous polyamine-based DES system was identified.

2. Experimental

2.1. Materials

Monoethanolamine (MEA, 99%, CAS No. 141-43-5, Macklin Biochemical Co. Ltd., China), diethylenetriamine (DETA, 99%, CAS No. 111-40-0, Macklin Biochemical Co. Ltd., China), piperazine (Pz, 99%, 110-85-0, Sigma-Aldrich, UAS), and hydrochloric acid (HCl, 35%, CAS No. 7647-01-0, VMR chemicals, USA) were used in this study. The CO_2 gas ($\geq$ 99%) was purchased from the AGA Linde Group. Ultrapure water produced by the Mili-QR ultrapure water system was used for synthesis and making aqueous mixtures.

2.2. Absorbent synthesis and characterization

Initially, Pz was protonated by HCl in an aqueous solution, which was achieved by mixing Pz dissolved in H_2O with equimolar aqueous

HCl solution. Following this, the solvent is removed through rotary evaporation and subsequent vacuum drying, yielding a white solid product, PzCl. Afterward, PzCl was mixed with DETA in a certain molar ratio, and then the mixture was stirred at 60 °C for 1 h till thorough homogenization, which allows for the efficient interaction between PzCl and DETA, to finally form anhydrous PD solutions. The chemical structures of HBA and HBD are shown in Fig. 1. The aqueous PD solutions were prepared by blending PD with H_2O at a certain mass fraction.

The density and viscosity of absorbents were tested using a digital density meter (DMA 4100 M) and a rolling-ball viscometer (Lovis 2000 ME) (both from Anton Paar, Austria) with an accuracy of 0.0001 g/cm^3 and 0.001 mPa·s, respectively. In the measurements, each sample was repeated at least three times, and the average value was reported with uncertainties of $u_r(\eta) \approx 0.015$ in viscosity and $u_r(\rho) \approx 0.02$ in density. Fourier transform infrared spectroscopy (FTIR) (VERTEX 70v, Bruker, Germany) was applied for characterizing the chemical composition and chemical bonds. Thermogravimetric analysis (TGA) was conducted using a simultaneous thermal analyzer (SDT Q600, TA Instruments, USA), in which the samples were heated from 40 to 500 °C at a rate of 10 °C/min under continuous N_2 flow.

2.3. CO_2 absorption and desorption experiments

2.3.1. CO_2 absorption at atmospheric pressure

The CO_2 absorption at atmospheric pressure was carried out using a gravimetric method [27,28]. Firstly, about 7 g absorbents (*i.e.*, the solvents of aqueous DES solutions or aqueous MEA solution) were added into a custom-made absorption bottle with an inner diameter of 2.0 cm, which was placed in a water bath at a controlled temperature, and then CO_2 was introduced into the absorbents at a flow rate of 100 mL/min. Absorption equilibrium was considered to be reached when there was no further increase in the mass. In the experiments, the water loss from the absorbents was assessed under identical experimental conditions and found to be negligible. The CO_2 absorption capacity was determined by monitoring the mass change of the system, which was recorded periodically using an electronic analytical balance with an accuracy of ±0.1 mg. The CO_2 absorption rate was determined by the relationship between the CO_2 capacity and time based on the kinetic model established in previous research [12].

$$r_t = -\frac{dn_t}{dt} \tag{1}$$

where n_t represents the CO_2 capacity (g-CO_2/g-absorbent) at time t.

2.3.2. CO_2 desorption experiment

The desorption process was carried out using the atmospheric pressure heating method [29], with the apparatus shown in Fig. 2. The experiment was carried out in a three-neck flask containing the CO_2-saturated absorbent, which was heated to 110 °C in an oil bath. The mixture was stirred continuously at 150 r/min. A serpentine condenser, maintained at 2 °C, was used to recover the water vapor released alongside the CO_2. Afterward, the concentrated sulfuric acid was employed to eliminate the residual moisture from the gas stream.

The CO_2 released rate (Q_t) was periodically recorded using a soap film flowmeter, and the corresponding CO_2 desorption rate (r_d, mol-

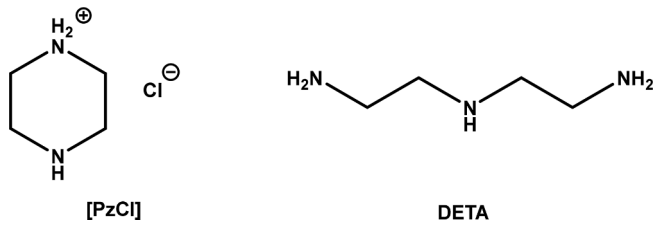

Fig. 1. Chemical structures of HBA and HBD.

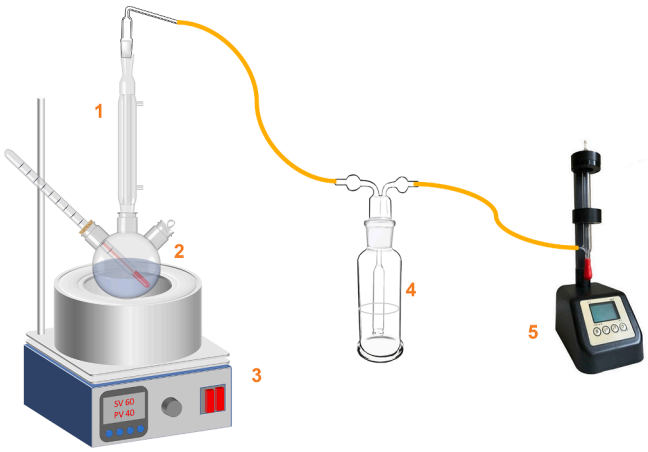

Fig. 2. CO_2 desorption experimental setup diagram (1. Condenser; 2. Three-necked flask; 3. Constant temperature oil bath; 4. Gas scrubber bottle with concentrated sulfuric acid; 5. Soap film flowmeter).

CO_2/(kg-absorbent·min)) was determined through Eq. (2), while the CO_2 desorbed amount (n_d) was calculated by integrating r_d over time, as shown in Eq. (3). Cycle-loading represented the total desorbed CO_2 (n_c), and the desorption efficiency (η) was determined based on cycle-loading and the saturated CO_2 capacity, following the formulation in Eq. (4).

$$r_d = \frac{Q_t \cdot M_{CO_2}}{m_s \cdot 22.4 \cdot 1000}\left(\frac{P(T_0+273.15)}{P_0(T+273.15)}\right) \tag{2}$$

$$n_d = \int_0^t r_d dt \tag{3}$$

$$\eta = \frac{n_c}{n_e} \cdot 100\% \tag{4}$$

where M_{CO2} represents the molecular weight of CO_2; P and T denote the actual pressure (0.1 MPa) and temperature (22 °C); P_0 and T_0 refer to the standard pressure (0.1 MPa) and temperature (0 °C); m_s is the mass of the absorbent; n_e is the saturated CO_2 capacity. All the above absorption and desorption experiments were performed at least three times, and the relative standard deviation (RSD) was controlled within 3% to ensure the data reliability.

3. Results and discussion

3.1. DESs characterization

In this section, we systematically investigated the thermal stability and chemical structure of PD using TGA and FTIR. The thermal decomposition temperature (T_d) was defined as the temperature at which a 5 wt% mass loss occurs. As shown in Fig. 3a, the T_d of Pz was found to be 68 °C, whereas its chlorinated derivative, PzCl, exhibited a significantly enhanced thermal stability with a decomposition temperature of 155 °C. DETA exhibited a decomposition temperature of 86 °C. Upon forming DESs by mixing PzCl and DETA at molar ratios of 1:4, 1:5, and 1:6, their T_d became 116, 112, and 103 °C, respectively. This implies that the incorporation of even a low PzCl content is sufficient to increase the thermal decomposition temperature of the DES, and higher PzCl content result in more stable DES systems, likely due to the formation of a hydrogen bonding network between PzCl and DETA, which strengthens the intermolecular forces and enhances the resistance to thermal degradation. Fig. 3b presents the FTIR spectra of the raw materials and PD with different molar ratios. A noticeable increase in the broad peak intensity within the 3000~3500 cm^{-1} region was observed, confirming the existence of the hydrogen bonds [12]. As displayed in Fig. 3c and 3d, the FTIR spectra of the aqueous DESs in the

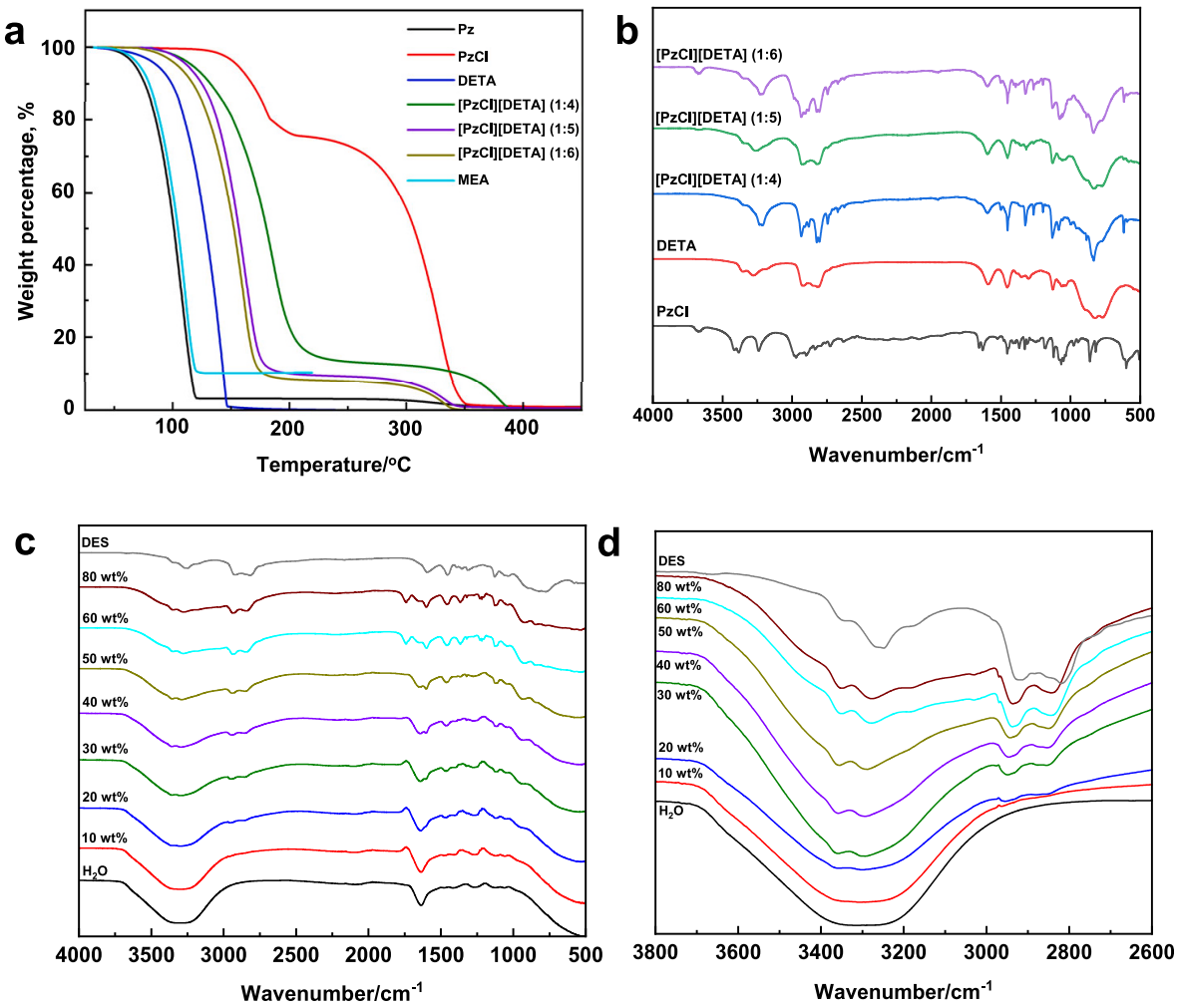

Fig. 3. (a) TGA and (b) FTIR spectra of anhydrous PD with different molar ratios; FTIR spectra of aqueous PD solutions with different PD contents in the range of (c) 500~4000 cm^{-1} and (d) 2600~3800 cm^{-1}.

2600~3800 cm^{-1} region reveal that, even at higher water contents, the characteristic hydrogen-bonding features of the DES are preserved. The gradual shift and broadening of the hydrogen bonds and stretching bands with increasing water content indicate enhanced hydrogen-bond interactions rather than disrupting the original DES network. When the water content was up to 80 wt%, the spectra remained distinguishable from the pure H_2O, suggesting the persistence of the DES-specific interactions.

3.2. *Optimizing molar ratio of PzCl to DETA*

Previous studies have shown that anhydrous DESs exhibit significantly high viscosity after the CO_2 absorption, rendering them impractical for industrial applications [12]. To address this issue, H_2O has been introduced as a co-solvent to effectively reduce viscosity while maintaining the intrinsic hydrogen bonding network and structural integrity of DESs. In order to systematically evaluate the absorption and desorption performance of the DESs in different molar ratios and the link to their properties, the PD content was fixed at 30 wt% in this section, and their performance was compared with that of 30 wt% MEA to assess their potential for industrial applications.

3.2.1. *Physical property*

The density and viscosity of absorbents, as well as the viscosity after the CO_2 absorption (*i.e.*, CO_2 saturated solutions), were investigated. The results are displayed in Fig. 4. As shown in Fig. 4a, the viscosity of the absorbent decreases with increasing temperature and decreasing the DETA content, whereas the density decreases with increasing temperature and increasing the DETA content. When the molar ratio of HBA to HBD changes from 1:4 to 1:6, the viscosity at 20 °C increases from 4.36 to 5.10 mPa·s, while the density decreases from 1.023 to 1.020 g/cm^3. This behavior can be attributed to the increased proportion of DETA, which enhances the hydrogen bonding network, resulting in stronger intermolecular interactions, and reduces the molecular mobility, thereby increasing the viscosity. Furthermore, the intensified hydrogen bonding network and increased structural complexity may lead to an expansion of intermolecular voids, reducing the number of molecules per unit volume and consequently lowering the density [30,31]. Fig. 4b illustrates the viscosity variations of aqueous PD solutions with different ratios before and after the CO_2 absorption, compared with the viscosity of 30 wt% MEA solution. The experimental results demonstrate that the viscosity of all samples increases after the CO_2 absorption. Although the post-absorption viscosity of aqueous PD solutions is slightly higher than that of 30 wt% MEA, it remains below 10 mPa·s, indicating favorable viscosity properties suitable for industrial applications.

3.2.2. *Absorption and desorption performance*

Fig. 5a illustrates the CO_2 absorption capacity of aqueous PD solutions and MEA solutions over time. The results demonstrate that the aqueous PD solutions achieves absorption capacities of 0.159, 0.168, and 0.176 g-CO_2/g-absorbent, significantly surpassing that of 30 wt% MEA (0.126 g-CO_2/g-absorbent). In Fig. 5a and 5b, if the saturation

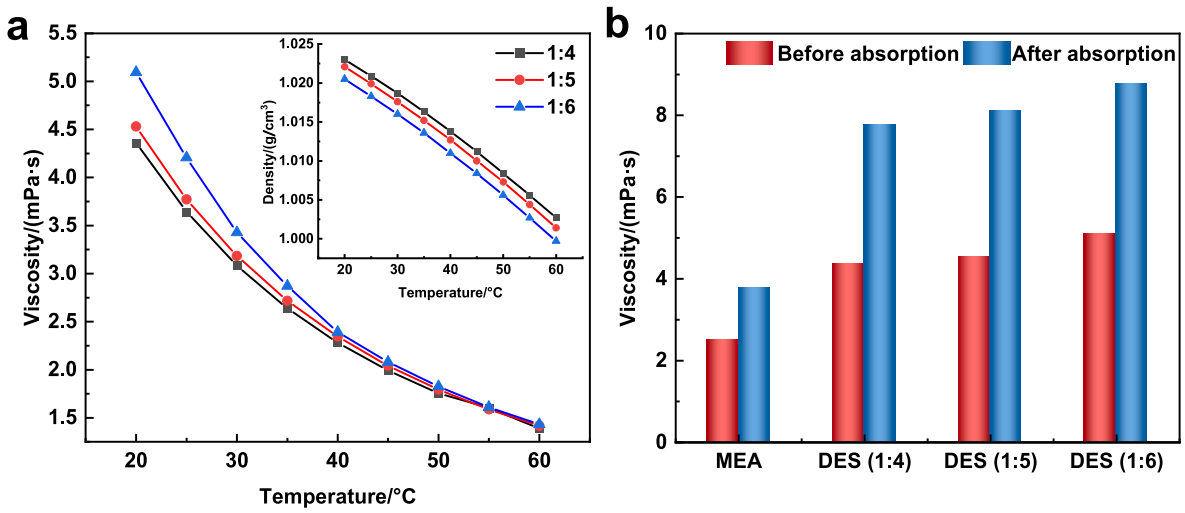

Fig. 4. (a) Variation of density and viscosity with temperature; (b) viscosity comparison before and after the CO_2 absorption (*i.e.*, CO_2-saturated solvents) at 20 °C and 0.1 MPa.

absorption time (T_{sat}) was defined as the time when the slope of the absorption curve reaches zero, as well as the point where the absorption rate becomes zero, it can be seen that all aqueous PD solutions reach saturation within 30 min, similar to the MEA aqueous, indicating remarkably high absorption efficiency. A comparison of the aqueous PD solutions with different ratios reveals that the absorption capacity increases with increasing the DETA content. This enhancement is attributed to DETA acting as the HBD, providing key active sites for the CO_2 capture. As the DETA proportion rises, the density of the active sites increases, leading to greater CO_2 binding capacity and enhancing the overall absorption performance. Fig. 5b presents the absorption rates of both aqueous PD and MEA solutions over time. The absorption rate peaks within the first 1∼2 min, followed by a gradual decline. This behavior can be explained by two primary factors: initially, the concentration of active sites is at its highest, enabling rapid CO_2 uptake. However, as the reaction proceeds, the number of available active sites diminishes [12]. Additionally, the viscosity of the solution increases due to the CO_2 binding, creating greater mass transfer resistance and resulting in a gradual decrease in the absorption rate. The peak absorption rates reach 0.51, 0.54, and 0.53 mol-CO_2/(kg-absorbent·min), which are comparable to 30 wt% MEA (0.53 mol-CO_2/(kg-absorbent·min)), highlighting the promising potential of aqueous PD solutions for industrial CO_2 capture applications.

The desorption behavior was evaluated by measuring the time-dependent CO_2 desorption rate, the desorbed CO_2 amount, and the CO_2 desorption efficiency at 110 °C and 0.1 MPa. Fig. 5c illustrates the desorption rate profiles of aqueous PD solutions and MEA solutions over time. The desorption rate of aqueous PD solutions initially peaks within the first 2∼5 min, indicating a rapid CO_2 release driven by the high driving force at the beginning of the process. Subsequently, the rate gradually declines due to the reduced CO_2 partial pressure difference and the depletion of readily desorbable CO_2 molecules. Compared to 30 wt% MEA (0.160 mol-CO_2/(kg-absorbent·min)), aqueous PD solutions exhibit 51%∼64% faster peak desorption rate (0.242∼0.262 mol-CO_2/(kg-absorbent·min)), suggesting improved kinetics, *i.e.*, faster regeneration. The aqueous PD solutions with different molar ratios exhibit distinct desorption kinetic characteristics. Increasing the DETA content reduces the time required to reach the peak desorption rate and enhances the peak desorption rate. This enhancement is primarily attributed to the higher initial CO_2 loading concentration. However, during the desorption rate decline phase, aqueous PD (1:4) solution exhibits a higher desorption rate than aqueous PD (1:6) solution. Furthermore, Fig. 5d depicts the desorbed CO_2 amount as a function of time for aqueous PD and MEA solutions. The aqueous PD solutions with molar ratios of 1:4, 1:5, and 1:6 achieve desorption amounts of 0.092, 0.090, and 0.082 g-CO_2/g-absorbent, which are 58%, 53%, and 39% higher than 30 wt% MEA (0.059 g-CO_2/g-absorbent). The desorption efficiencies were further calculated by Eq. (4), with values of 57%, 54%, and 47%, respectively.

In summary, the results demonstrate that an increase in the PzCl content enhances the desorption rate in the rate decline phase, desorption amount, and desorption efficiency, further highlighting the pivotal role of PzCl in the aqueous PD systems. On the one hand, the presence of PzCl weakens the interactions between the absorbent and CO_2, thereby reducing the CO_2 binding strength and facilitating its release. On the other hand, the unique physicochemical properties of ILs, including low volatility, high thermal stability, and desirable proton transfer ability, reduce the solvent pyrolysis and volatilization during the desorption and thus optimize the desorption process [15].

3.2.3. *Global comparison*

Table 1 summarizes the CO_2 absorption-desorption performance and key physical properties of aqueous PD solutions with different HBA:HBD ratios, revealing the comprehensive influence of the DETA content. The analysis shows the following trends: as the DETA proportion increases, the CO_2 absorption capacity improves due to the increased availability of active sites in DETA, which enhances the chemical absorption. However, this increase comes with notable trade-offs, including a rise in pre- and post-absorption viscosity, likely attributed to the formation of more complex hydrogen bonding networks, reducing fluidity. Additionally, the reduced desorption amount and desorption efficiency suggest that a higher DETA content intensifies CO_2 binding strength, impeding CO_2 release. Coupled with the TGA analysis in section 3.1, a higher DETA ratio also results in a reduction in T_d, indicating compromised thermal stability. Considering the balance among absorption capacity, desorption performance, viscosity, and thermal stability, the PD with an HBA:HBD ratio of 1:5 was selected as the optimal candidate for subsequent studies, aiming to achieve improved absorption-desorption performance.

3.3. *Optimizing PD content*

In order to optimize the composition of aqueous PD solutions for CO_2 capture, the impact of the PD content in the aqueous solutions on the physicochemical properties and the absorption-desorption performance was systematically investigated in this section.

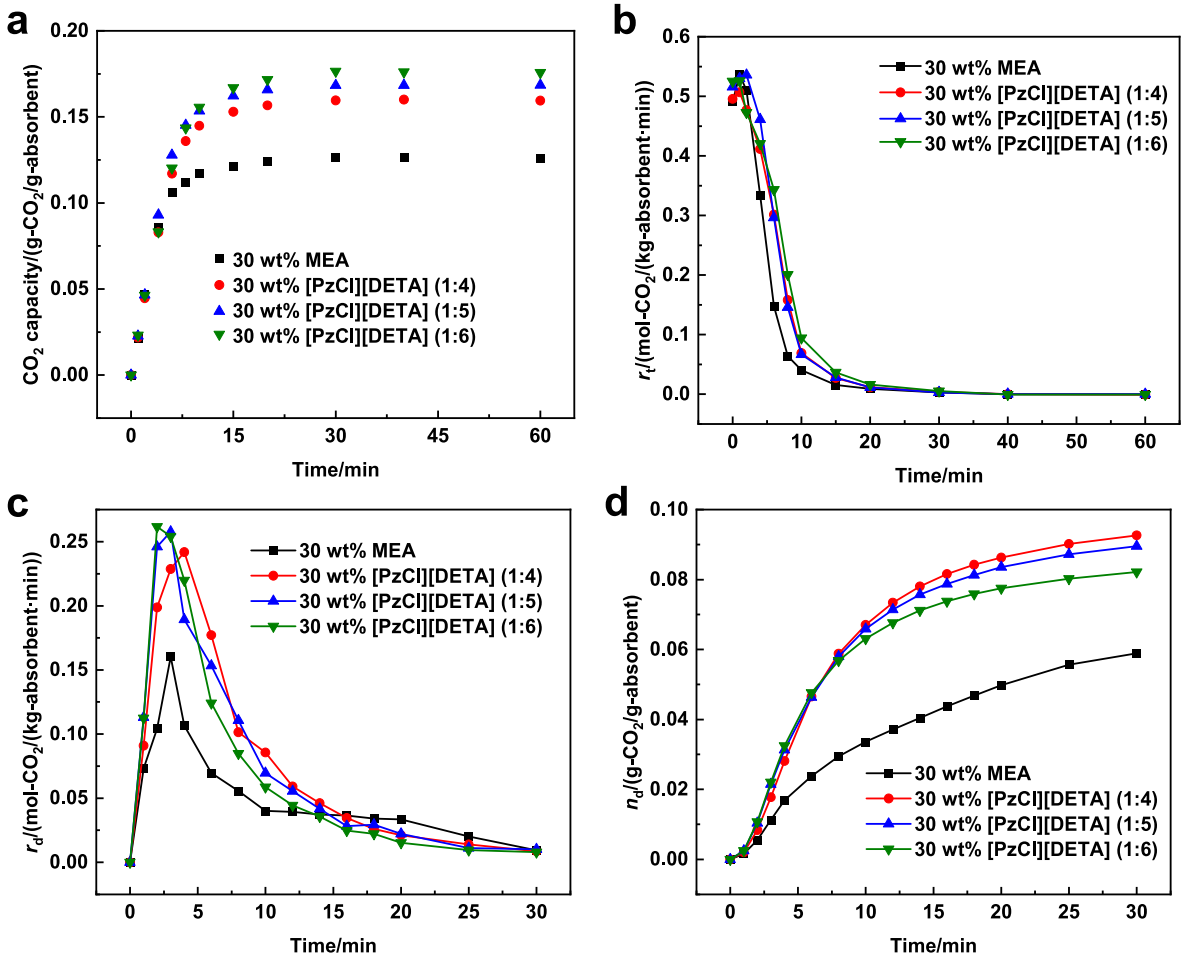

Fig. 5. (a) CO_2 absorption capacity, (b) CO_2 absorption rate, (c) CO_2 desorption rate, and (d) CO_2 desorption amount curves of 30 wt% MEA and 30 wt% PD solutions with different molar ratios of HBA to HBD (absorption at 22 °C and 0.1 MPa, desorption at 110 °C and 0.1 MPa).

Table 1
Properties and performance of 30 wt% PD and 30 wt% MEA.

Absorbent	Viscosity/(mPa·s)		Capacity/(g-CO_2/g-absorbent)		T_{sat} /min	η, %
	Before	After	n_e	n_d		
MEA	2.49	3.77	0.126	0.059	30	47
PD (1:4)	4.36	7.77	0.160	0.092	30	57
PD (1:5)	4.53	8.11	0.168	0.090	30	54
PD (1:6)	5.10	8.77	0.176	0.082	30	47

3.3.1. *Physical property*

Fig. 6a shows the viscosity and density of aqueous PD solutions at various temperatures and PD contents. As depicted, both the viscosity and density of the aqueous PD solutions decrease with increasing temperature and decreasing the PD content. When the temperature increases from 20 to 60 °C, the viscosities of 20 wt%, 30 wt%, 40 wt%, and 60 wt% PD in H_2O range from 2.46 to 0.93, 4.53 to 1.42, 9.98 to 2.49, and 61.99 to 6.51 mPa·s, respectively. It indicates a significant rise in the initial viscosity before CO_2 absorption as the PD content increases. The densities of aqueous PD solutions follow a linear trend with temperature. Furthermore, as the PD content rises from 20 wt% to 60 wt%, the density at 20 °C increases from 1.01 to 1.05 g/cm^3.

Fig. 6b illustrates the variation in viscosity of the aqueous PD solutions before and after the CO_2 absorption (*i.e.*, CO_2-saturated solvents). A noticeable increase in viscosity was observed across all absorbents, with the extent of the increase positively correlated with the PD content. Specifically, the viscosity of 20 wt% PD increases from 2.46 to 3.86 mPa·s, marking a 57% rise; 30 wt% PD rises from 4.53 to 8.11 mPa·s (79% increase); 40 wt% PD elevates from 9.98 to 28.13 mPa·s, achieving a 182% increment. Notably, 60 wt% PD exhibits a drastic surge from 61.99 to 1362 mPa·s, escalating by 21-fold. This trend highlights that a higher PD concentration leads to a more pronounced viscosity growth after the CO_2 absorption. This phenomenon can be attributed to the greater production of the carbamate species at the high PD content. These products tend to gather in the absorbent, making hydrogen bonds stronger and increasing the interactions between molecules. Consequently, the molecular mobility in the solution is significantly hindered, resulting in a substantial rise in viscosity [31,32]. It is obvious that when the PD content reaches 60 wt%, the resulting viscosity becomes excessively high, posing significant limitations for industrial applications due to hindered mass transfer and increased operational costs.

3.3.2. *Absorption and desorption performance*

The absorption capacity curves displayed in Fig. 7a reveal that the CO_2 uptake increases progressively with increasing the PD contents, indicating an enhanced availability of the active sites provided by PD. The saturated absorption capacities for 20 wt%, 30 wt%, 40 wt%, and 60 wt% PD are 0.116, 0.168, 0.217, and 0.283 g-CO_2/g-absorbent, respectively, demonstrating that, except for 20 wt% PD, the capacities show significant improvement compared to the benchmark 30 wt% MEA solution. T_{sat} increases with rising the PD content, as observed when the PD content increases from 20 wt% to 60 wt%, resulting in an increase from 20 to 60 min. This is primarily due to the inherently high viscosity

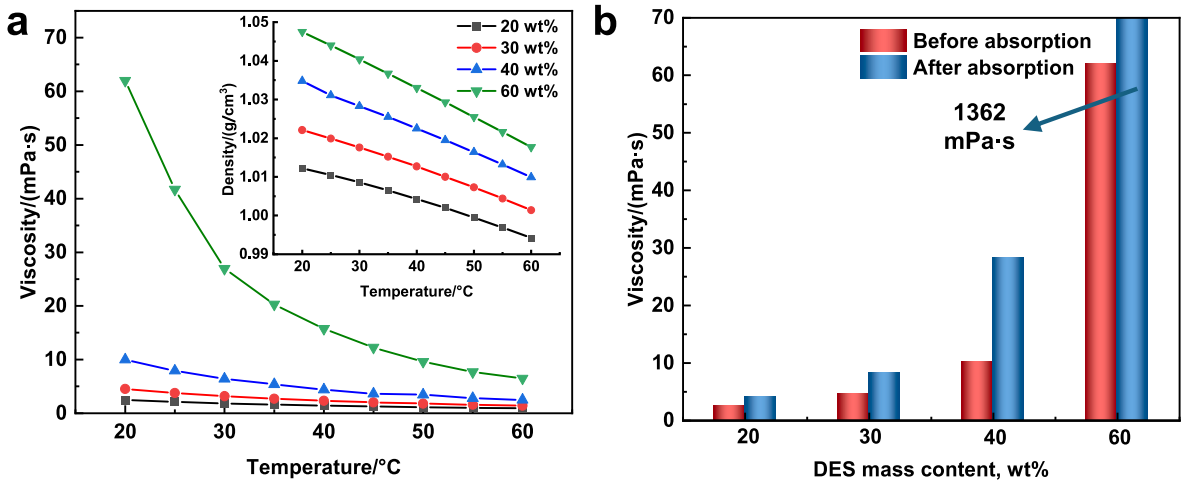

Fig. 6. (a) Variation of density and viscosity with temperature; (b) viscosity comparison before and after the CO_2 absorption (*i.e.*, CO_2-saturated solvents) at 20 °C and 0.1 MPa.

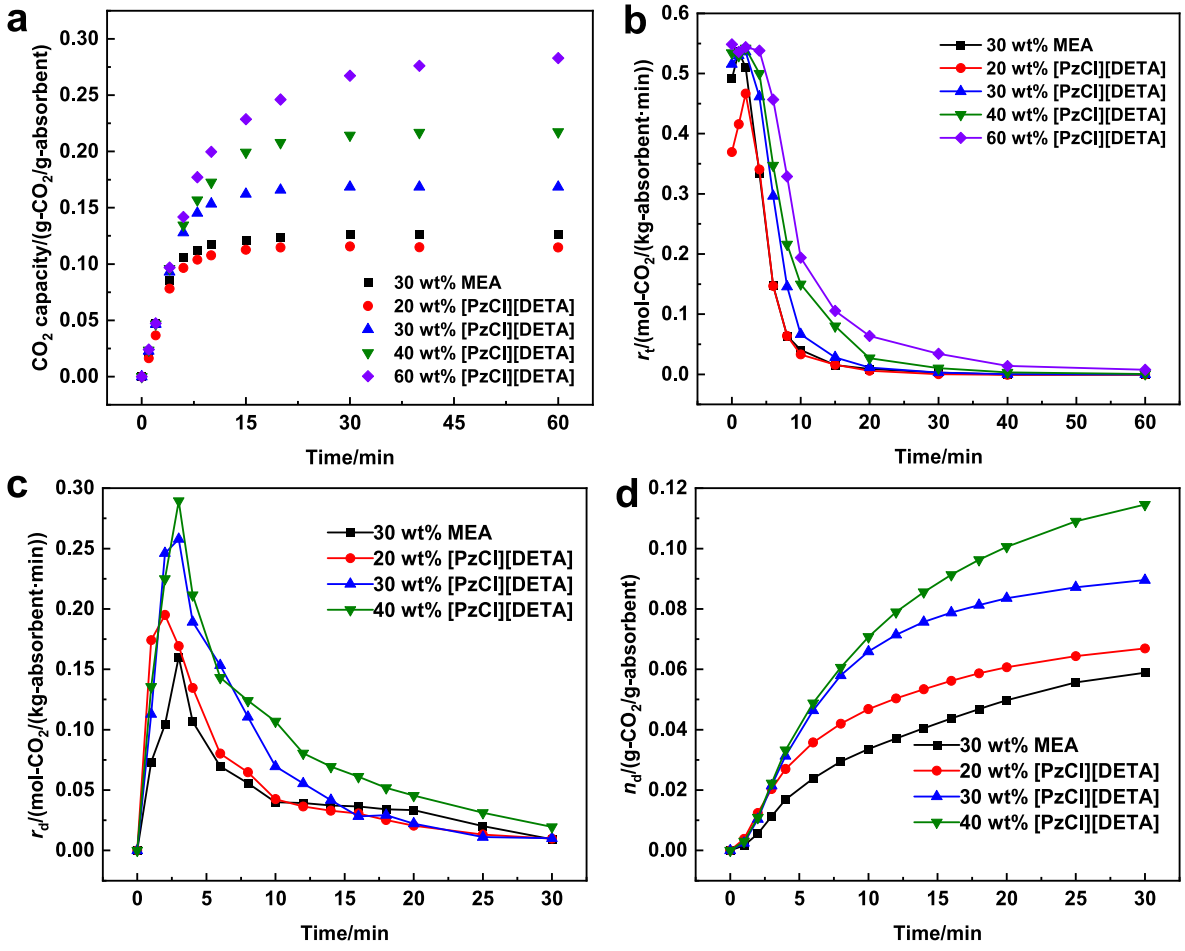

Fig. 7. (a) CO_2 absorption capacity, (b) CO_2 absorption rate, (c) CO_2 desorption rate, and (d) CO_2 desorption amount curves of 30 wt% MEA and PD (1:5) with different water contents (absorption at 22 °C and 0.1 MPa, desorption at 110 °C and 0.1 MPa).

of the absorbent with a high PD content, coupled with the continuous increase in viscosity during the absorption process as CO_2 is absorbed and products are formed. The escalating viscosity hinders mass transfer during the later stages of the absorption, thereby slowing down the overall absorption process and extending the time required to reach the CO_2 saturation.

The absorption rate curves displayed in Fig. 7b reveal that the initial absorption rate of the aqueous PD solutions increases as the PD content increases, reaching 0.369, 0.516, 0.534, and 0.548 mol-CO_2/(kg-absorbent·min) for 20 wt%, 30 wt%, 40 wt%, and 60 wt% PD solutions, respectively. A significant increase of 40% is observed when the PD concentration increases from 20 wt% to 30 wt%. However, the growth

becomes less pronounced (only 6%) as the concentration rises from 30 wt% to 60 wt%. This suggests that the enhanced initial absorption rate from 20 wt% to 30 wt% PD is predominantly driven by the increased active site density, facilitating more rapid CO_2 capture. However, with further concentration increases, the significant rise in viscosity becomes the primary limiting factor for the absorption rate. As a result, despite the continued increase in the active site density, the initial absorption rate no longer exhibits a substantial improvement. A similar trend is observed in the maximum absorption rate, where solutions with 30~60 wt% PD exhibit a comparable peak absorption rate of about 0.540 mol-CO_2/(kg-absorbent·min), approximately 16% higher than that of 20 wt% PD (0.466 mol-CO_2/(kg-absorbent·min)). During the subsequent deceleration phase, the absorption rate consistently follows the pattern of 60 wt% > 40 wt% > 30 wt% > 20 wt% in PD. This behavior can be attributed to the faster depletion of active sites in the low-concentration of PD, leading to an earlier equilibrium state. Higher PD concentrations, despite increased viscosity, sustain a higher absorption rate for a longer duration due to the greater availability of active sites at the start of the process.

Considering the excessively high viscosity of 60 wt% PD after the CO_2 absorption, further investigation into its desorption performance was deemed impractical. Therefore, the desorption behaviors of 20 wt%, 30 wt%, and 40 wt% PD were analyzed. As illustrated in Fig. 7c, 20 wt% PD achieves its peak desorption rate of 0.195 mol-CO_2/(kg-absorbent·min) within 2 min, while 30 wt% and 40 wt% PD solutions reach their peak desorption rates of 0.258 and 0.289 mol-CO_2/(kg-absorbent·min), respectively, within the first 3 min. This upward trend in peak desorption rate with increasing the PD concentration can be attributed to the higher CO_2 loading of absorbents at elevated PD concentrations. The greater CO_2 content provides a larger reservoir of releasable CO_2, and under the high temperature conditions, the differences in viscosity among the absorbents are less pronounced, facilitating faster desorption at higher PD concentrations.

As shown in Fig. 7d, the total desorption amounts for 20 wt%, 30 wt %, and 40 wt% PD were 0.067, 0.090, and 0.114 g-CO_2/g-absorbent, respectively, demonstrating an upward trend with increasing the PD concentration. This increase in desorption capacity is attributed to the higher initial CO_2 loading in the absorbent at elevated PD concentrations, providing a larger reservoir of releasable CO_2 during the desorption process. However, the desorption efficiency decreased from 58% to 54% and 52% as the PD concentration increased from 20 wt% to 30 wt% and 40 wt%, respectively. This phenomenon can be attributed to the increased PD content, which raises the concentrations of both the raw materials and the CO_2-bound products in the absorbent, enhancing the complexity of the hydrogen bond network among various compounds. Consequently, a greater amount of energy and a longer duration may be required to disrupt this more complex hydrogen bond network, which in turn hinders the efficient desorption of CO_2.

3.3.3. Global comparison

To comprehensively evaluate the CO_2 capture performance of aqueous PD solutions with various PD contents, key indicators were analyzed as displayed in Table 2, including pre- and post-absorption viscosity, CO_2 absorption capacity, absorption saturation time, CO_2 desorption amount, and desorption efficiency. A balanced absorbent must exhibit low viscosity for efficient mass transfer, high CO_2 uptake, rapid absorption rates, as well as high desorption amount and efficiency for effective regeneration. For the 20 wt% PD, notable advantages were observed in viscosity and desorption efficiency. However, its CO_2 absorption capacity remained relatively low, falling below the conventional 30 wt% MEA solution. In contrast, 40 wt% PD demonstrated a significantly higher absorption capacity than 30 wt% MEA. Nevertheless, its post-absorption viscosity surged to 28.13 mPa·s, which far exceeds the desirable industrial threshold of 10 mPa·s for effective mass transfer performance, rendering it less practical for large-scale applications. On this basis, 30 wt% PD emerged as a balanced candidate, achieving an absorption capacity of 0.168 g-CO_2/g-absorbent, 34% higher than 30 wt% MEA. Moreover, it exhibited a higher absorption

Table 2
Properties and performance of aqueous PD solutions with different PD contents.

Absorbent	Viscosity/(mPa·s)		Capacity/(g-CO_2/g-absorbent)		T_{sat}/min	η, %
	Before	After	n_e	n_d		
30 wt% MEA	2.49	3.77	0.126	0.059	30	47
20 wt% PD	2.46	3.86	0.114	0.067	20	58
30 wt% PD	4.53	8.11	0.168	0.090	30	54
40 wt% PD	9.98	28.13	0.217	0.114	40	52

Table 3
Comparison of the CO_2 capacity and viscosity of different DESs.

DES	H_2O content, wt%	T/P (°C/MPa)	Viscosity/(mPa·s)		Capacity/(g-CO_2/g-absorbent)	Ref.
			Before	After		
[PzCl][DETA] (1:5)	60	22/0.1	9.98	28.13	0.54	This work
[PzCl][DETA] (1:5)	70	22/0.1	4.53	8.11	0.56	
[PzCl][DETA] (1:5)	80	22/0.1	2.46	3.86	0.57	
[TEPACl][MEA] (1:2)	20	25/0.015	117.96	–	0.41	[4]
[TEPACl_2][MEA] (1:4)	20	25/0.015	39.78	–	0.47	
[TEPACl_3][MEA] (1:6)	20	25/0.015	37.47	–	0.23	
[MEACl][MEA] (1:6)	0	40/0.8	29	–	0.092	[18]
[MEACl][DETA] (1:6)	0	40/0.8	14	–	0.242	
[MEACl][EDA] (1:6)	0	40/0.8	9	–	0.327	
[ChCl][TEA] (1:4)	0	25/10	–	–	0.198	[33]
[MEACl][MDEA] (1:3)	0	25/0.1	–	–	0.116	[32]
[MEACl][MDEA][MEA] (1:3:0.5)	0	25/0.1	–	–	0.135	
[MEACl][EDA] (1:5)	60	22/0.1	5.27	16.16	0.383	[12]
[MEACl][EDA] (1:5)	50	22/0.1	9.22	59.82	0.43	

Table 4
Performance of 30 wt% PD at different temperatures.

Temperature/°C	n_e (g-CO_2/g-absorbent)	T_{sat}/min	Rate/(mol-CO_2/(kg-absorbent·min))	
			r_i	r_p
22	0.168	30	0.516	0.536
40	0.166	20	0.805	0.836
50	0.162	20	0.804	0.904
60	0.152	10	0.809	0.832
80	0.136	10	0.493	0.626

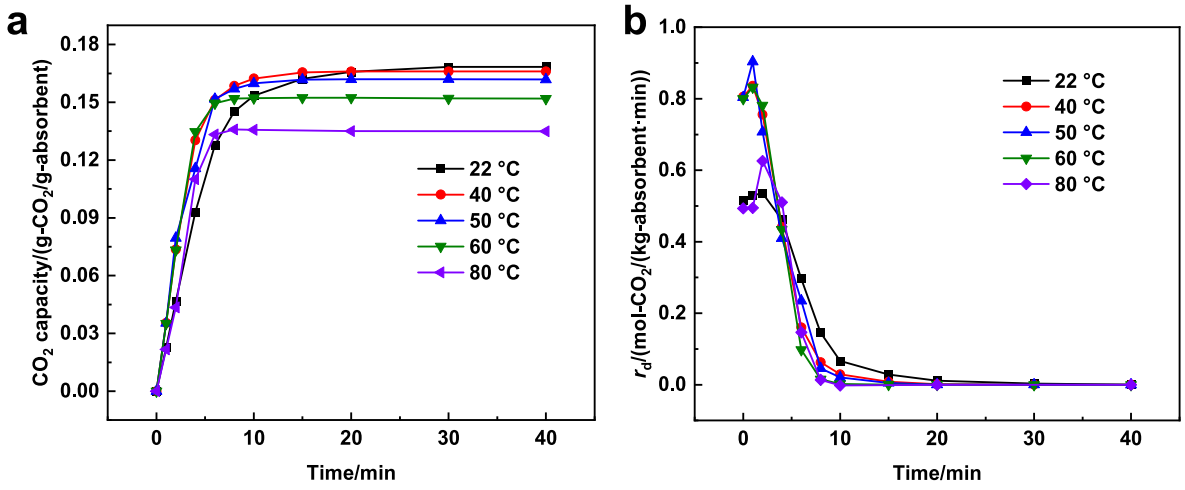

Fig. 8. (a) CO_2 absorption capacity and (b) CO_2 absorption rate curves of 30 wt% PD at different temperatures and 0.1 MPa.

rate comparable to that of the 40 wt% PD while maintaining a more manageable post-absorption viscosity of 8.11 mPa·s and a desorption efficiency of 54%. This optimal trade-off among absorption capacity, desorption performance, and viscosity makes 30 wt% PD a promising and viable choice for industrial applications.

To better assess the potential of the DES identified in this work, a comparative analysis was conducted between the absorption performance and physical properties of our system and those reported in the literature as shown in Table 3. The comparison demonstrates that, compared with many reported DESs that suffer from either low absorption capacity or a dramatic viscosity increase after CO_2 loading, 30 wt% [PzCl][DETA] presents a favorable balance between the absorption efficiency and manageable viscosity.

3.4. *Effect of temperature on CO_2 capture*

The effect of temperature on the CO_2 absorption performance of 30 wt% PD was systematically examined at 22, 40, 50, 60, and 80 °C by analyzing both the absorption capacity and absorption rate, as shown in Fig. 8 and Table 4. The results reveal a distinct temperature dependence in CO_2 absorption capacity, which exhibits minimal variation (0.168~0.162 g-CO_2/g-absorbent) when the temperature ranges from 22 to 50 °C; but declines significantly (0.162~0.136 g-CO_2/g-absorbent) as the temperature further increases from 50 to 80 °C. Fig. 8b indicates that the absorption rates at 22 and 80 °C are much lower than those at other temperatures, which implies that the absorption rate decreases at both extremely high and low temperatures. This is because the effect of temperature on the CO_2 absorption rate is influenced by a combination of viscosity, molecular kinetic energy, and reaction equilibrium constant. As the temperature increases, the viscosity of aqueous PD decreases and molecular kinetic energy increases, facilitating CO_2 diffusion and enhancing chemical reaction rate. However, since CO_2 absorption is an exothermic process, higher temperatures shift the reaction equilibrium toward the reverse direction, therefore reducing the thermodynamic driving force. As a result, the overall reactivity of aqueous PD solution to CO_2 decreases, leading to a reduction in absorption rate at extremely high temperatures.

4. Conclusions

This study demonstrates the significant potential of aqueous polyamine-based DES systems for efficient CO_2 capture, while highlighting critical trade-offs between the absorption capacity, desorption efficiency, and viscosity. Firstly, the influence of the PzCl/DETA molar ratios on the physicochemical properties, structure characters, and CO_2 absorption/desorption behavior was systematically examined. The findings revealed that increasing the proportion of PzCl enhanced the thermal stability of anhydrous [PzCl][DETA] and improved desorption efficiency, as well as reduced post-absorption viscosity of aqueous [PzCl][DETA]. Conversely, a high DETA proportion increased the CO_2 absorption capacity. Balancing multiple performance factors, [PzCl][DETA] (1:5) was determined to be the optimal DES. To further elucidate how the [PzCl][DETA] content affects CO_2 absorption-desorption performance, aqueous [PzCl][DETA] solutions with the PD contents of 20 wt%, 30 wt%, and 40 wt% were investigated. The results demonstrated that elevated [PzCl][DETA] concentrations resulted in significantly enhanced absorption capacities (0.114~0.217 g-CO_2/g-absorbent), while concurrently prolonging the saturation absorption time (20~40 min), increasing the post-absorption viscosity (3.86~28.13 mPa·s), and diminishing the desorption efficiency (58%~52%). Among them, 30 wt% [PzCl][DETA] exhibited a superior CO_2 capacity of 0.168 g-CO_2/g-absorbent while maintaining a more manageable post-absorption viscosity of 8.11 mPa·s and a desorption efficiency of 54%, so it was identified to be the optimal absorption system. The insights gained from this study contribute to a deep understanding of the DES system and its potential for advancing efficient and sustainable carbon capture technologies.

CRediT authorship contribution statement

Kaige Jia: Writing – original draft, Methodology, Data curation. **Qiangbing Shi:** Writing – review & editing, Methodology. **Xiaoyan Ji:** Writing – review & editing, Supervision, Funding acquisition.

Declaration of competing interests

X. Ji is an editorial board member of *Green Chemical Engineering* and is not involved in the editorial review or the decision to publish this article. The authors declare that they have no known competing financial interests or personal relationships that could have appeared to influence the work reported in this paper.

Acknowledgements

This work was financially supported by the European Union, Grant Agreement No. 101146861 (NIAGARA) and the Swedish Energy Agency (Energimyndigheten) (P2023-00911).

References

[1] D. Garza, P. Dargusch, D. Wadley, A technological review of direct air carbon capture and storage (DACCS): global standing and potential application in Australia, Energies 16 (2023) e4090.

[2] A.A. Bodour, N. Alomari, A. Gutiérrez, S. Aparicio, M. Atilhan, Exploring the thermophysical properties of natural deep eutectic solvents for gas capture applications: a comprehensive review, Green Chem. Eng. 5 (2024) 307–338.

[3] H.C. Lau, S.C. Tsai, Global decarbonization: current status and what it will take to achieve net zero by 2050, Energies 16 (2023) e7800.

[4] J. Ju, D. Choi, S. Cho, Y. Yoo, D. Kang, Absorption characteristics and rheological properties of quaternized polyamine-based deep eutectic solvents for high performance CO_2 capture, Chem. Eng. J. 496 (2024) e153922.

[5] G. Cui, J. Wang, S. Zhang, Active chemisorption sites in functionalized ionic liquids for carbon capture, Chem. Soc. Rev. 45 (2016) 4307–4339.

[6] G. Cui, Y. Cheng, W. Zhang, X. Shen, L. Li, R. Zhang, Y. Chen, Q. Ke, C. Ge, H. Liu, W. Fan, H. Lu, Highly efficient CO_2 capture from open air and dilute gas streams by tunable azolate ionic liquids based deep eutectic solvents, Chem. Eng. J. 505 (2025) e159193.

[7] K. Rigkos, G. Filis, I. Antonopoulou, A. De Oliveira Maciel, P. Saridis, D. Zarafeta, G. Skretas, Biomimetic CO_2 capture unlocked through enzyme mining: discovery of a highly thermo- and alkali-stable carbonic anhydrase, Environ. Sci. Technol. 58 (2024) 17732–17742.

[8] J. Wang, Z. Song, L. Chen, T. Xu, L. Deng, Z. Qi, Prediction of CO_2 solubility in deep eutectic solvents using random forest model based on COSMO-RS-derived descriptors, Green Chem. Eng. 2 (2021) 431–440.

[9] Y. Liu, Z. Dai, Z. Zhang, S. Zeng, F. Li, X. Zhang, Y. Nie, L. Zhang, S. Zhang, X. Ji, Ionic liquids/deep eutectic solvents for CO_2 capture: reviewing and evaluating, Green Energy Environ. 6 (2021) 314–328.

[10] F. Erek, M.F. Lanjwani, M. Tuzen, A sensitive determination of brilliant blue FCF in some food samples using hydrophilic deep eutectic solvent-assisted magnetic nano gel-based dispersive solid phase microextraction prior to spectrophotometric analysis, Food Chem. 453 (2024) e139632.

[11] F. Gabriele, M. Chiarini, R. Germani, M. Tiecco, N. Spreti, Effect of water addition on choline chloride/glycol deep eutectic solvents: characterization of their structural and physicochemical properties, J. Mol. Liq. 291 (2019) e111301.

[12] S. Foorginezhad, X. Ji, Development of monoethanolamine chloride-ethylene diamine deep eutectic solvent for efficient carbon dioxide capture, Sep. Purif. Technol. 347 (2024) e127593.

[13] M. Yan, Q. Huan, Y. Zhang, W. Fang, F. Chen, A. Pariatamby, E. Kanchanatip, H. Wibowo, Effect of operating parameters on CO_2 capture from biogas with choline chloride—monoethanolamine deep eutectic solvent and its aqueous solution, Biomass Conv. Bioref. 14 (2024) 283–297.

[14] Y. Zhang, R. Han, S. Zhou, X. Wang, J. Zhao, Y. Zhang, L. Wang, X. Sun, L. Xia, S. Xiang, Amine-based deep eutectic solvents for CO_2 capture: experiments and molecular thermodynamics, Sep. Purif. Technol. 359 (2025) e130559.

[15] F. Meng, T. Ju, S. Han, L. Lin, J. Li, K. Chen, J. Jiang, Novel monoethanolamine absorption using ionic liquids as phase splitter for CO_2 capture in biogas upgrading: high CH_4 purity and low energy consumption, Chem. Eng. J. 462 (2023) e142296.

[16] N. Altunay, M.F. Lanjwani, H.U. Haq, M. Tuzen, A. Elik, Sensitive method for determination of benzoic acid in beverages and food samples using air–assisted hydrophobic deep eutectic solvent-based dispersive liquid-liquid microextraction, Sustain. Chem. Pharm. 38 (2024) e101464.

[17] N. Altunay, A. Elik, M. Farooque Lanjwani, M. Tuzen, Assessment of arsenic in water, rice and honey samples using new and green vortex-assisted liquid phase microextraction procedure based on deep eutectic solvent: multivariate study, Microchem. J. 179 (2022) e107541.

[18] K.A. Pishro, G. Murshid, F.S. Mjalli, J. Naser, Investigation of CO_2 solubility in monoethanolamine hydrochloride based deep eutectic solvents and physical properties measurements, Chin. J. Chem. Eng. 28 (2020) 2848–2856.

[19] Y. Zhang, Y. Song, H. Jin, T. Wu, H. Xiao, Y. Xiang, J. Yun, L. Shao, Study on CO_2 absorption by novel choline chloride-diethylenetriamine-water deep eutectic solvents in a rotor-stator reactor, Chem. Eng. Process. Process Intensif. 184 (2023) e109299.

[20] M.A. Kassim, N.A. Sulaiman, R. Yusoff, M.K. Aroua, Non-aqueous solvent mixtures for CO_2 capture: choline hydroxide-based deep eutectic solvents absorbent performance at various temperatures and pressures, Sustainability 15 (2023) e9191.

[21] R. Biswas, A.K. Metya, K.M. Abebe, S.A. Gedf, B.T. Melese, Carbon dioxide solubility in choline chloride-based deep eutectic solvents under diverse conditions, J. Mol. Model. 29 (2023) e236.

[22] M. Aboshatta, V. Magueijo, A comprehensive study of CO_2 absorption and desorption by choline-chloride/levulinic-acid-based deep eutectic solvents, Molecules 26 (2021) e5595.

[23] Bhawna, A. Pandey, S. Pandey, Superbase-added choline chloride-based deep eutectic solvents for CO_2 capture and sequestration, ChemistrySelect 2 (2017) 11422–11430.

[24] M. Lu, G. Han, Y. Jiang, X. Zhang, D. Deng, N. Ai, Solubilities of carbon dioxide in the eutectic mixture of levulinic acid (or furfuryl alcohol) and choline chloride, J. Chem. Thermodyn. 88 (2015) 72–77.

[25] Y. Du, Y. Wang, G.T. Rochelle, Piperazine/4-hydroxy-1-methylpiperidine for CO_2 capture, Chem. Eng. J. 307 (2017) 258–263.

[26] C. Yang, T. Li, P. Tantikhajorngosol, T. Sema, M. Xiao, P. Tontiwachwuthikul, Evaluation of novel aqueous piperazine-based physical-chemical solutions as biphasic solvents for CO_2 capture: initial absorption rate, equilibrium solubility, phase separation and desorption rate, Chem. Eng. Sci. 277 (2023) e118852.

[27] S. Foorginezhad, X. Ji, Developing non-aqueous slurry for CO_2 capture, Carbon Capture Sci. Technol. 15 (2025) e100385.

[28] K. Jia, S. Zeng, G. Li, W. Liu, Y. Bai, X. Zhang, T. Wang, M. Fang, Impurities effect on CO_2 capture from flue gas by energy-efficient diazole-functionalized ionic liquid solvents, Sep. Purif. Technol. 358 (2025) e130270.

[29] L. Xiao, Z. Qiu, S. Feng, X. Duan, Z. Zhao, Y. Liu, L. Ma, Carbon dioxide absorption and desorption experiments based on MDEA, Chem. Eng. Process. Process Intensif. 204 (2024) e109931.

[30] Z. Zuo, B. Cao, L. Lu, X. Lu, X. Ji, Thermodynamic study of ionic liquids 1-hexyl-3-methylimidazolium halide with methanol mixtures, J. Chem. Eng. Data 69 (2024) 3392–3402.

[31] Z. Zuo, X. Lu, X. Ji, Modeling the viscosity of ionic liquids and their mixtures using ePC-SAFT and free volume theory with an ion-based approach, Ind. Eng. Chem. Res. 64 (2025) 2446–2464.

[32] N. Ahmad, X. Lin, X. Wang, J. Xu, X. Xu, Understanding the CO_2 capture performance by MDEA-based deep eutectics solvents with excellent cyclic capacity, Fuel 293 (2021) e120466.

[33] T. Altamash, M. Atilhan, A. Aliyan, R. Ullah, M. Nasser, S. Aparicio, Rheological, thermodynamic, and gas solubility properties of phenylacetic acid-based deep eutectic solvents, Chem. Eng. Technol. 40 (2017) 778–790.